Acta Mechanica Solida Sinica, Vol. 28, No. 5, October, 2015 ISSN 0894-9166
Published by AMSS Press, Wuhan, China

UNCERTAINTY ANALYSIS OF ROCK FAILURE BEHAVIOUR USING AN INTEGRATION OF THE PROBABILISTIC COLLOCATION METHOD AND ELASTO-PLASTIC CELLULAR AUTOMATON**

Pengzhi Pan[1⋆] **Fangsheng Su**[1] **Haijun Chen**[2] **Shilin Yan**[2] **Xiating Feng**[1] **Fei Yan**[1]
([1] *State Key Laboratory of Geomechanics and Geotechnical Engineering, Institute of Rock and Soil Mechanics, Chinese Academy of Sciences, Wuhan* 430071*, China*)
([2] *School of Science, Wuhan University of Technology, Wuhan* 430071*, China*)

Received 22 October 2013, revision received 16 December 2014

ABSTRACT The Karhunen-Loeve (KL) expansion and probabilistic collocation method (PCM) are combined and applied to an uncertainty analysis of rock failure behavior by integrating a self-developed numerical method (i.e., the elastic-plastic cellular automaton (EPCA)). The results from the method developed are compared using the Monte Carlo Simulation (MCS) method. It is concluded that the method developed requires fewer collocations than MCS method to obtain very high accuracy and greatly reduces the computational cost. Based on the method, the elasto-plastic and elasto-brittle-plastic analyses of rocks under mechanical loadings are conducted to study the uncertainty in heterogeneous rock failure behaviour.

KEY WORDS uncertainty analysis, probabilistic collocation method, elasto-plastic cellular automaton, Karhunen-Loeve expansion, rock failure process, PCM-EPCA

I. INTRODUCTION

The heterogeneity of rocks is an important cause for the complexity of their mechanical behaviour. The mechanical parameters of rocks show great heterogeneity and anisotropy in space, which directly affects their mechanical behaviour and leads to uncertainty. Uncertainty analysis is therefore meaningful and of theoretical value.

In past decades and with the development of computational techniques, random theory and methods were gradually introduced for the analysis of random systems. Many stochastic approaches have been developed[1–11] to study the effect of spatial variability on the physical behaviour (e.g., subsurface flow) of rock masses. The Monte Carlo Simulation (MCS) method is the most popular used to solve random problems[12, 13]. However, it requires a large number of samples to reach convergence. The technique is generally used to provide benchmark solutions for assessing the accuracy of other stochastic approaches due to its easy implementation[7, 14]. An alternative to MCS simulation is the moment equation method[15], which derives a system of deterministic differential equations that govern the statistical moments of the random variables. However, the computational cost of the conventional moment equation method

⋆ Corresponding author. E-mail: pzpan@whrsm.ac.cn

** Project supported by the National Natural Science Foundation of China (Nos. 51322906 and 41272349), the National Basic Research Program of China (No. 2013CB036405) and Youth Innovation Promotion Association of CAS (No. 2011240).

is high for large-scale problems. A moment equation approach based on the Karhunen-Loeve (KL) expansion was proposed for single-phase, unsaturated and multiphase flows[8, 14, 16]. Another approach called the polynomial chaos expansion (PCE) method has aroused considerable interest in quantifying uncertainty in various mechanics problems[17]. However, the deterministic coefficients of the PCE are governed by a set of coupled equations, which are difficult to solve when the number of coefficients is large. Furthermore, the simulators used in deterministic simulations cannot be directly employed since the original governing equations are coupled to PCE coefficients. The probabilistic collocation method (PCM) introduced by Tatang et al.[18] is another efficient stochastic approach. This method uses PCEs to represent the random variables of interest. A collocation technique is used instead of the Galerkin scheme to solve PCE coefficients prior to deriving independent deterministic equations.

Other methods, such as the moment equation method, KL moment equation, probabilistic collocation method, random finite element method, etc., are used by researchers to reduce the computational costs and guarantee accuracy. Of these methods, the PCM is widely used because of its unique characteristics for solving random problems.

Moreover, the traditional deterministic mechanical model we used does not perfectly agree with practice. Therefore, research into uncertainty problems has important practical and theoretical values. We introduce both the random field theory and the methods required to characterise the complex mechanical behaviour of rocks. Therefore, the current aim is to combine stochastic analytical methods with geotechnical engineering numerical simulations while considering the variability of the mechanical rock parameters in the spatial domain. Furthermore, it is necessary to establish both the suitable stochastic analytical theory and the corresponding calculation methods for geotechnical engineering. This paper addresses a method for studying the uncertainty of rock failure behaviour using a combination of PCM and a self-developed numerical code (i.e., the elasto-plastic cellular automaton (EPCA)[19, 20]). The integration of these two methods and their associated applications are demonstrated.

II. PROBABILISTIC COLLOCATION METHOD

In rock engineering, probabilistic problems can be expressed using the following random differential equation:

$$K(u, \varpi(x, \theta))u = F(\theta) \tag{1}$$

where K is a random coefficient matrix. u is the target of the problem. $F(\theta)$ is the random external force. $\varpi(x, \theta)$ represents the random material properties. θ is a random event and x is an independent variable.

The PCM is implemented using the following steps:

(1) Representation of random input field

In this work, we use KL expansion to represent the input field based on a set of independent standard random variables. Consider the following random input domain:

$$Y(X, \theta) = \ln \varpi(X, \theta) \quad (X \in D, \quad \theta \in \Omega) \tag{2}$$

where D is the physical domain, and Ω is the probability space.

The mean value is assumed to be the following:

$$\bar{Y}(X) = \langle Y(X, \theta) \rangle \tag{3}$$

The covariance of $Y(X, \theta)$ is as follows:

$$C_Y(X_1, X_2) = \left\langle \left[Y(X_1, \theta) - \bar{Y}(X_1) \right] \left[Y(X_2, \theta) - \bar{Y}(X_2) \right] \right\rangle \tag{4}$$

For two arbitrary points, $X_1 = \{x_{11},\, x_{12},\, x_{13}\}^{\mathrm{T}}$, $X_2 = \{x_{21},\, x_{22},\, x_{23}\}^{\mathrm{T}}$, in domain D, the covariance function can be expressed in the Gaussian form

$$C_Y(X_1, X_2) = \sigma_Y^2 \exp\left[-\frac{\pi}{4} \sum_{i=1}^{3} \left(\frac{x_{1i} - x_{2i}}{\lambda_i} \right)^2 \right] \tag{5}$$

where σ_Y^2 is the variance, and λ_i is the autocorrelation length.

As the covariance equation is symmetrical and positive, it can be divided as follows:

$$C_Y(X_1, X_2) = \sum_{i=1}^{\infty} \eta_i f_i(X_1) f_i(X_2) \tag{6}$$

where η_i is the eigenvalue of covariance function, and $f(X)$ is the eigenfunction, which can be solved using the Fredholm integral equation of the second kind:

$$\int_D C_Y(X_1, X_2) f_i(X_2) \mathrm{d}X_2 = \eta_i f_i(X_1) \tag{7}$$

The random domain, $Y(X, \theta)$, can be divided into a mean value $\bar{Y}(X)$ and residual part $Y'(X, \theta)$, which is represented by the KL expansion. Therefore, the random domain can be expressed as follows:

$$Y(X, \theta) = \bar{Y}(X) + Y'(X, \theta) = \bar{Y}(X) + \sum_{i=1}^{\infty} \xi_i(\theta) \sqrt{\eta_i} f_i(X) \tag{8}$$

where ξ_i is a standard set of orthogonal random variables that satisfy $< \xi_i >= 0$ and $< \xi_i \xi_j >= \delta_{ij}$.

When the eigenvalue is sorted as $\eta_1 \geq \eta_2 \geq \ldots$, the associated characteristic function is sorted in the same way. The attenuation rate of η_n determines the number of retained items, which determines the random dimension of the problem.

If the KL expansion is truncated at the N^{th} item, we have the following:

$$Y(X, \theta) = \bar{Y}(X) + Y'(X, \theta) = \bar{Y}(X) + \sum_{i=1}^{N} \xi_i(\theta) \sqrt{\eta_i} f_i(X) \tag{9}$$

$Y(X, \theta)$ approximates the weighted sum of N random variables $\xi_i \, (i = 1, 2, \cdots, N)$ using the eigenvalue and deterministic characteristic function.

(2) Representation of random output domain

In this work, we use PCE to describe the output field based on the standard random variables of the input field.

The random output domain depends on the input, and its function depends on the random vector $\xi = (\xi_1, \xi_2, \cdots, \xi_N)^{\mathrm{T}}$; where ξ_i is a random variable for an input parameter. The relation between the output domain and ξ should be determined. The random output domain cannot be represented by a KL expansion as its statistical characteristics are unknown. The PCE method is used to represent the output domain.

The output domain u is expressed using the following polynomials[21–23]:

$$\begin{aligned} u(X, t, \xi) = \; & a_0(X, t) + \sum_{i_1=1}^{\infty} a_{i_1}(X, t) \Gamma_1(\xi_{i_1}) + \sum_{i_1=1}^{\infty} \sum_{i_2=1}^{i_1} a_{i_1 i_2}(X, t) \Gamma_2(\xi_{i_1}, \xi_{i_2}) \\ & + \sum_{i_1=1}^{\infty} \sum_{i_2=1}^{i_1} \sum_{i_3=1}^{i_2} a_{i_1 i_2 i_3}(X, t) \Gamma_3(\xi_{i_1}, \xi_{i_2}, \xi_{i_3}) + \cdots \end{aligned} \tag{10}$$

where $a_0(X, t)$ and $a_{i_1 i_2 \ldots i_d}(X, t)$ are deterministic functions of X, and $\Gamma_d(\xi_{i1}, ..., \xi_{id})$ is a PCE of order d with respect to the independent random variables $(\xi_{i1}, ..., \xi_{id})$.

The above equation is the discrete version of the original Wiener polynomial chaos expansion, where continuous integrals are replaced by summations[24].

For independent standard Gaussian random variables, $\Gamma_d(\xi_{i1}, ..., \xi_{id})$ is expressed as follows:

$$\Gamma_d(\xi_{i1}, ..., \xi_{id}) = (-1)^d \mathrm{e}^{\xi^{\mathrm{T}} \xi / 2} \frac{\partial^d}{\partial \xi_{\xi_{i1} \ldots \xi_{id}}} (\mathrm{e}^{-\xi^{\mathrm{T}} \xi / 2}) \tag{11}$$

where $\xi = (\xi_{i1}, ..., \xi_{id})^{\mathrm{T}}$.

In practice, Eq.(10) is usually truncated to a finite number of terms, P, and can be simplified as follows:

$$\hat{u}(X, t, \xi) = \sum_{j=1}^{P} c_j(X, t) \Phi_j(\xi) \tag{12}$$

where ξ is a vector of dimension N. $\Phi_j(\xi)$ is a basis function. There is a one-to-one correspondence between the terms in Eq.(10) and those in Eq.(11). The total number of terms P is determined by the random dimensionality, N, and PCE degree,

$$P = 1 + \frac{N!}{(N-1)!} + \frac{(N+1)!}{(N-1)!2!} + \frac{(N+2)!}{(N-1)!3!} + \cdots + \frac{(N-1+d)!}{(N-1)!d!} = \frac{(N+d)!}{N!d!} \tag{13}$$

(3) Determining the PCE coefficients

Both the Galerkin scheme and the PCM are commonly used to determine the PCE coefficients that can be derived via the weighted residual method. In this work, the PCM is used to obtain random solutions from random space.

If the solution of a non-linear random differential equation is $u = u(X, t, \xi)$, the residual R is defined as follows:

$$R_p(X, t, \xi) = u(X, t, \xi) - \hat{u}(X, t, \xi) \tag{14}$$

Letting $R_p(X, t, \xi) = 0$ yields the following:

$$\sum_{j=1}^{P} \{\Phi_k \Phi_j K[u, \exp(\bar{Y}(X) + \sum_{i=1}^{N} \xi_i(\theta)\sqrt{\eta_i} f_i(X))]\} C_j(X, t) = (\Phi_k F(\theta)) \quad (k = 1, 2, \cdots, P) \tag{15}$$

For each position X in space and t in time, P linear equations and p unknowns, $C_j(X, t)$, are formulated. The coefficients $\Phi_j(\xi^i)$ at the collocation point ξ^i can be calculated in advance. By solving this linear equation, the coefficients in the PCE can be determined from their position and time.

Compared to the Galerkin scheme, the PCM creates non-coupling equations that can be solved using other numerical methods. Therefore, the PCM is suitable for solving linear and non-linear problems.

(4) Evaluation of the output statistical behaviour

An important feature of the PCE is that its polynomial items are orthogonal,

$$\langle \Phi_i(\xi) \Phi_j(\xi) \rangle = 0 \quad (i \neq j) \tag{16}$$

if $i = j$, $\langle \Phi_j^2 \rangle$ can be easily calculated.

The following is the mean value of the output domain:

$$\bar{\hat{u}}(X, t, \xi) = \langle \hat{u}(X, t, \xi) \rangle = \sum_{j=1}^{P} c_j(X, t) \langle \Phi_j(\xi) \rangle = c_1(X, t) \tag{17}$$

The variance of the output domain can be expressed as follows:

$$\begin{aligned} \sigma_{\hat{u}}^2 &= \left\langle [\hat{u}(X, t, \xi) - \langle \hat{u}(X, t, \xi) \rangle]^2 \right\rangle = \sum_{j=2}^{P} \sum_{k=2}^{P} c_j(X, t) c_k(X, t) \langle \Phi_j(\xi) \Phi_k(\xi) \rangle \\ &= \sum_{j=2}^{P} c_j^2(X, t) \langle \Phi_j^2 \rangle \end{aligned} \tag{18}$$

where $\langle \Phi_j^2 \rangle$ can be calculated in advance.

(5) Determination of the collocation point

When implementing the PCM, an important step is determining the collocation point. For an order-specified PCE approximation, each collocation point can be selected from the orthogonal polynomial roots.

For example, the coordinate collocation points for second order Hermit PCEs can be chosen from the root of the third-order Hermite polynomial, $\xi^3 - 3\xi$ (i.e., $-\sqrt{3}, 0, \sqrt{3}$). Each collocation point is a combination of these three roots. Two illustrative collocation points are listed below:

$$\xi^1 = (\xi_1^1, \xi_2^1, ..., \xi_N^1)^{\mathrm{T}} = (0, 0, ..., 0)^{\mathrm{T}} \quad \text{and} \quad \xi^2 = (\xi_1^2, \xi_2^2, ..., \xi_N^2)^{\mathrm{T}} = (\sqrt{3}, 0, ..., 0)^{\mathrm{T}}$$

The number of collocation points equals the number of coefficients to be determined Eq.(13).

III. ELASTO-PLASTIC CELLULAR AUTOMATON

The elasto-plastic cellular automaton (EPCA)[19, 20] is a numerical model that simulates the failure process in heterogeneous rocks. This model conveniently considers the heterogeneity of the rock mass. The completely nonlinear failure process of rocks from a load to failure can be traced. This model is based on the localisation theory since it uses the cellular automaton technique. The local mechanical behaviour can be updated within the failure process.

In the EPCA, the rock behaviour is governed by a rotating Mohr-Coulomb fracture model, which is able to simulate rock fracturing from both tension and compression forces. For the tension, the Rankine failure criterion is defined as follows:

$$\sigma_i - \sigma_t = 0 \quad (i = 1, 2, 3) \tag{19}$$

where σ_t is the tensile strength. For the compression, the Mohr-Coulomb failure criterion is defined by the following:

$$|\tau| = c - \sigma_n \tan\phi = c - \sigma_n \mu \tag{20}$$

where c is the cohesion strength, ϕ is the internal friction angle, and μ is the coefficient of friction. To model the hardening, perfect plasticity, softening and brittle behaviours in rock (Fig.1(a)), the material strength parameters were defined as functions of the equivalent plastic strains (Fig.1(b)):

$$\bar{\varepsilon}^{\mathrm{p}} = \int \sqrt{\frac{2}{3}\left(\mathrm{d}\varepsilon_1^{\mathrm{p}}\mathrm{d}\varepsilon_1^{\mathrm{p}} + \mathrm{d}\varepsilon_2^{\mathrm{p}}\mathrm{d}\varepsilon_2^{\mathrm{p}} + \mathrm{d}\varepsilon_3^{\mathrm{p}}\mathrm{d}\varepsilon_3^{\mathrm{p}}\right)} \tag{21}$$

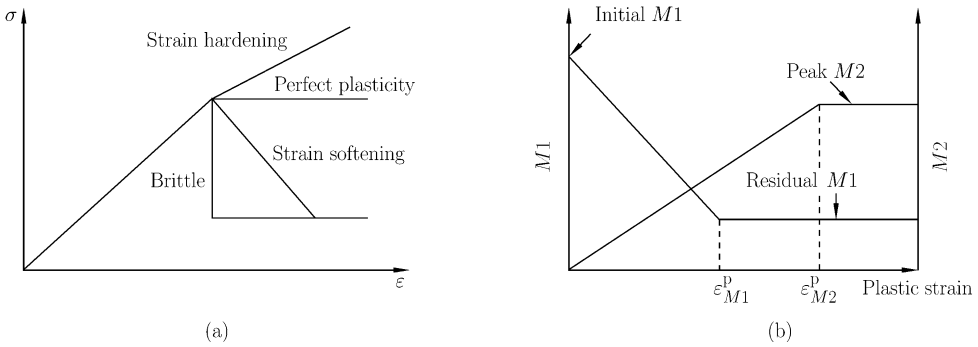

Fig. 1. (a) Constitutive relation and (b) parameters for the evolution rule.

The rock heterogeneity, which is a major factor in the complex failure of rocks, is considered by the EPCA code. The heterogeneity of the material data (such as Young's modulus, tensile strength, and cohesion) are used on an elemental level, which allows each element to have an independent value assigned to each property. The heterogeneity can be characterised using certain statistical approaches. For example, some researchers use a Weibull distribution to describe the material distribution parameters of the rocks[19]. In a Weibull distribution, two parameters are used to characterise the rock heterogeneity: (1) the homogeneous index, m, which represents the degree of material homogeneity, and (2) the elemental seed parameter, which controls the spatial variation of the other parameters.

By considering different homogeneous indices (i.e., m =1.1, 3.0, 5.0, 7.0) for rocks (random seed s = 10, which controls the spatial arrangement of parameters), the failure process of rocks uniaxial compression was studied to demonstrate the ability of the EPCA system to model the rock failure process. The size of the rock specimen is 100 mm×50 mm. The model was discretised into 5000 cell elements. The displacement loading control method was used with a loading speed of 0.005 mm/step. Table 1 shows the mechanical parameters used by the model.

Figure 2 shows the complete stress-strain curves for heterogeneous rocks with different homogeneous indices under uniaxial compression conditions. With increasing mechanical load, the heterogeneous rock specimen experiences several phases, such as a linear phase, a non-linear phase, strain softening, etc.

Table 1. **Rock mechanical parameters**

Parameters	Value	Parameters	Value
Young's modulus	48600 MPa	Cohesion	20 MPa
Poisson's ratio	0.24	Residual cohesion	1 MPa
Friction angle	49°	Tensile strength	8 MPa
Homogeneous index	1.1, 3.0, 5.0, 7.0	Residual tensile strength	0.1 MPa
Random seed	5, 10, 50, 100		

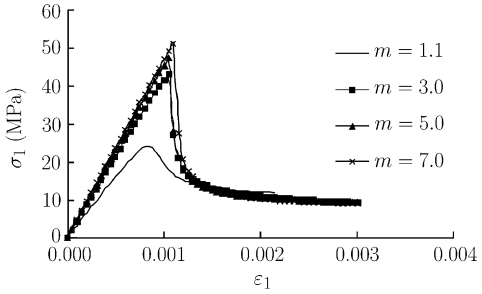

Fig. 2. Complete stress-strain curves for rock specimens with different homogeneous indices.

Figure 3 shows how the fracturing process is affected by different homogeneous indices. It was found that the failure process is greatly affected by the heterogeneity of the rocks (Fig.3).

The influence of the spatial arrangement of the parameters on the failure process was studied based on the different random seeds (s =5, 10, 50 and 100) of rocks ($m = 2.0$). The specimen and its associated mechanical parameters are the same as above.

Figures 4 and 5 show the complete stress-strain curves with the associated failure process for rocks with the same homogeneous index but differing spatial arrangements. In this case, the failure patterns of the rocks differ from one another. Similar stress-strain behaviour was found for each rock specimen.

The numerical results indicate the rock failure behaviour is greatly influenced by its heterogeneity. Heterogeneous rock specimens have different strengths, failure modes and deformation behaviours. Therefore, the rock failure behaviour presents a high uncertainty. However, in this section, only a few rock specimens were considered to represent finite situations in real world. In reality, the failure behaviour of rocks is more complex. Therefore, it is necessary to conduct uncertainty analysis on the rock failure behaviour.

IV. UNCERTAINTY ANALYSIS OF ROCK FAILURE BEHAVIOUR BASED ON PCM AND EPCA

1. Introduction to the integration of PCM and EPCA

PCM and EPCA are integrated to study the uncertainty in the failure processes of rocks. In this case, the mechanical parameters (e.g., stiffness or strength parameters) form the input random field. The output field can be the displacement, stress or plastic strain.

The procedure can be summarised as follows and shown in Fig.6:

(1) Let a random domain follow the normal distribution and then determine its mean and variance.

(2) Determine the probabilistic collocation points, P, which indicate how many times the EPCA will be called to generate the sample.

(3) Generate the first collocation points according to the elemental information and associated centre coordinates. A random sample of each mechanical property is produced according to the KL expansion.

(4) Call the EPCA system to calculate the mechanical behaviour of each sample with the input mechanical parameters.

(5) Repeat steps 3-4 until the total calculations are P.

(6) Post procedure. Each coefficient in the PCE can be determined using the data from P calculations. These results are saved and output.

For this model, parameters such as the unit correlation length (*etap*), mean value (*meany*), variance (*vary*), number of expansion and running times, etc., are required. The number of expansion items

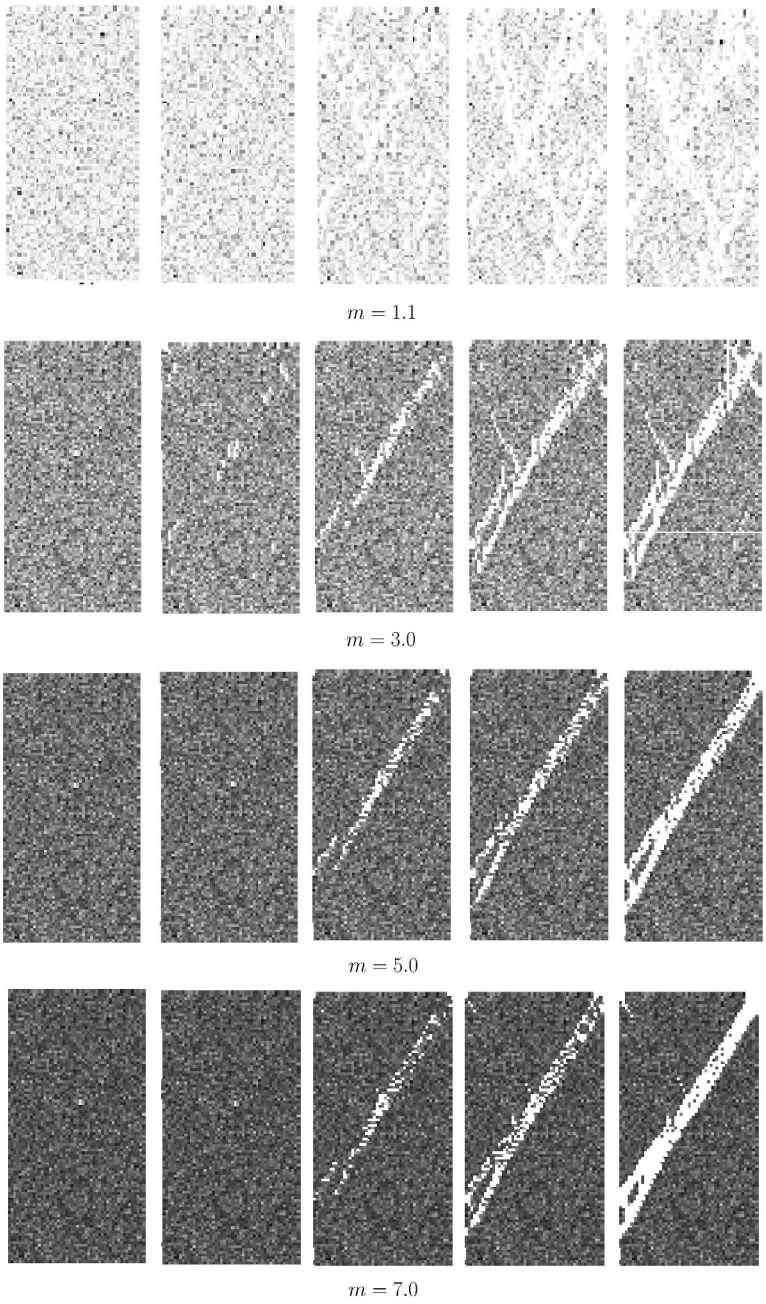

Fig. 3. Failure process for rocks with different homogeneous indices.

(nkl) is the number of items reserved in the KL expansion. The relation between the second-order PCM calculation time (npc) and the expansion is as follows:

$$npc = \frac{(nkl+2)(nkl+1)}{2} \tag{22}$$

Based on the above theories and procedures, a numerical system (i.e., the PCM-EPCA) is developed to analyse the uncertainty of heterogeneous rocks under a mechanical load involving the elastic analysis, elasto-plastic analysis and elasto-brittle-plastic analysis.

2. Elastic analysis

First, we consider a rock specimen with a size of 100 mm×50 mm discretised into a system composed of 200 cell elements. An external force ($F = 5 \times 10^5$ N) is applied to the middle of the upper boundary

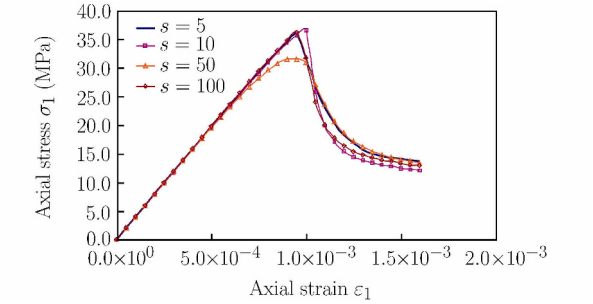

Fig. 4. Complete stress-strain curves for rock specimens with identical homogeneous indices but a different spatial random seed.

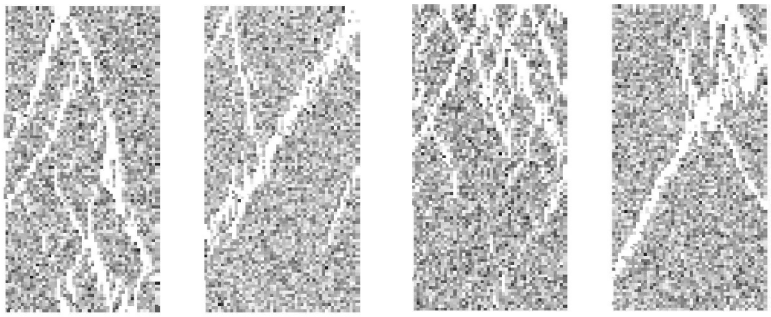

Fig. 5. Failure pattern for rock specimens with identical homogeneous indices but a different spatial random seed.

(Fig.7). In this section, we use Young's Modulus (E) as the random input field, and the governing equations are expressed as follows:

$$\begin{aligned} &\frac{E}{(1-\mu^2)}\left(\frac{\partial^2 u}{\partial x^2}+\frac{1-\mu}{2}\frac{\partial^2 u}{\partial y^2}+\frac{1+\mu}{2}\frac{\partial^2 v}{\partial x\partial y}\right)+X=0 \\ &\frac{E}{(1-\mu^2)}\left(\frac{\partial^2 v}{\partial y^2}+\frac{1-\mu}{2}\frac{\partial^2 v}{\partial x^2}+\frac{1+\mu}{2}\frac{\partial^2 u}{\partial x\partial y}\right)+Y=0 \end{aligned} \tag{23}$$

The displacement (u) is the estimated output field and is calculated as follows:

$$u=\sqrt{u_x^2+u_y^2} \tag{24}$$

The uncertainty analysis for the displacement of spatially heterogeneous rocks under a concentrated force is conducted using PCM-EPCA. For this model, the mean value of Young's Modulus is $\mu = 2.7\times10^8$ Pa, the variance is $\sigma^2 = 7.29\times10^{14}$ Pa^2, the standard deviation is $\sigma = 2.7\times10^7$ Pa, and the coefficient of variation is C.V. $= \sigma/\mu = 10\%$. Using a second-order PCM, we calculate the cases shown in Table 2.

Table 2. **Parameters for the second order PCM**

Case	*etap*	*meany* (Pa)	*vary* (Pa)^2	*nkl*	*npc*
1	0.4	2.7×10^8	7.29×10^{14}	5	21
2	0.4	2.7×10^8	7.29×10^{14}	10	66
3	0.4	2.7×10^8	7.29×10^{14}	20	231
4	0.4	2.7×10^8	7.29×10^{14}	30	496
5	0.4	2.7×10^8	7.29×10^{14}	40	861

According to Table 2, different second order expansion terms (i.e., *nkl* =5, 10, 20, 30, and 40, representing PCM-5, PCM-10, PCM-30, PCM-40 in the analyses, respectively) are considered. The mean

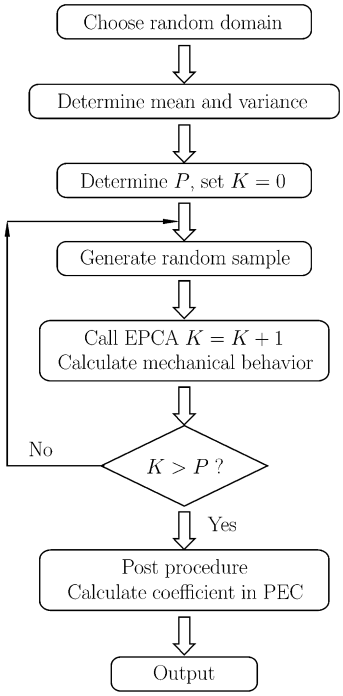

Fig. 6. Flow chart of the combination of PCM and EPCA.

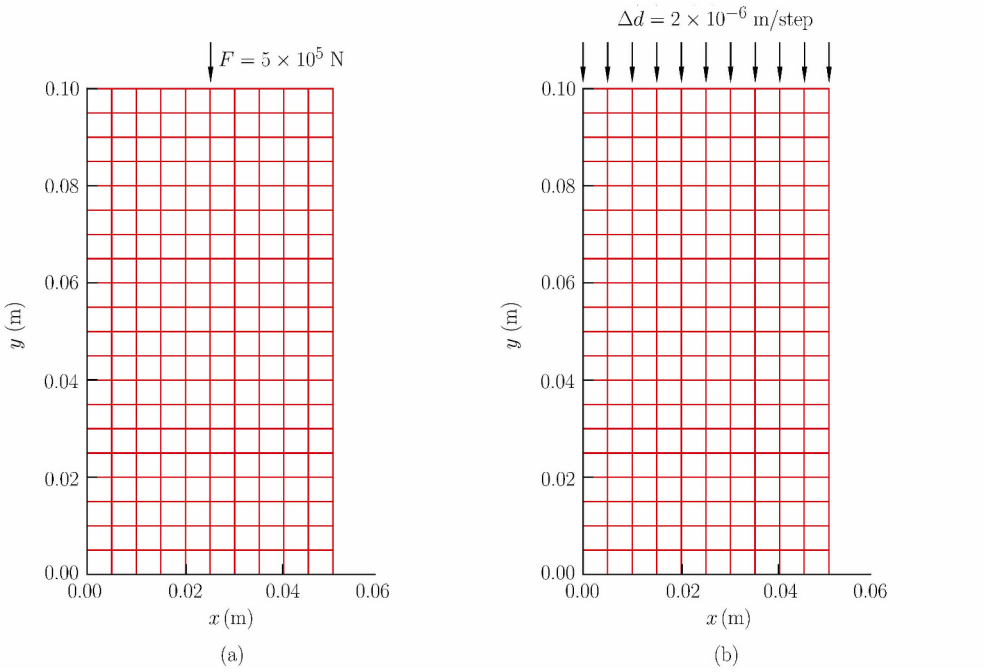

Fig. 7. Numerical model for (a) elastic analysis and (b) elasto-plastic and elasto-brittle-plastic analysis.

values and standard variances of the displacement fields are shown in Figs.8∼12, where mean represents the mean value and STD represents the standard variance. It is found that the mean displacement values obtained from the PCM model using different expansion terms have similar trends. Due to the application of a force concentrated on the top of the rock, a large displacement gradient is found. In the lower parts of the rock, the displacement is gentler. When the expansion term is above 20, the magnitude of the mean displacement remains nearly unchanged, as indicated by the displacement mean value contour.

The change in displacement of the STD fluctuates greatly at the top because of the concentrated force. In the lower part, the STD displacement is smaller. The calculation precision is not high enough for a second order PCM with 5 expansion terms because the number of calculations is only 21. As a result, the displaced STD is not consistent for the top of the model (Fig.8). Increasing the expansion term and calculation times causes the standard deviation contour to behave similarly. For random simulations, a second order PCM (i.e., nkl =20, 231 calculation times) is sufficient to guarantee the precision. The results change little when the expansion item is larger than 40.

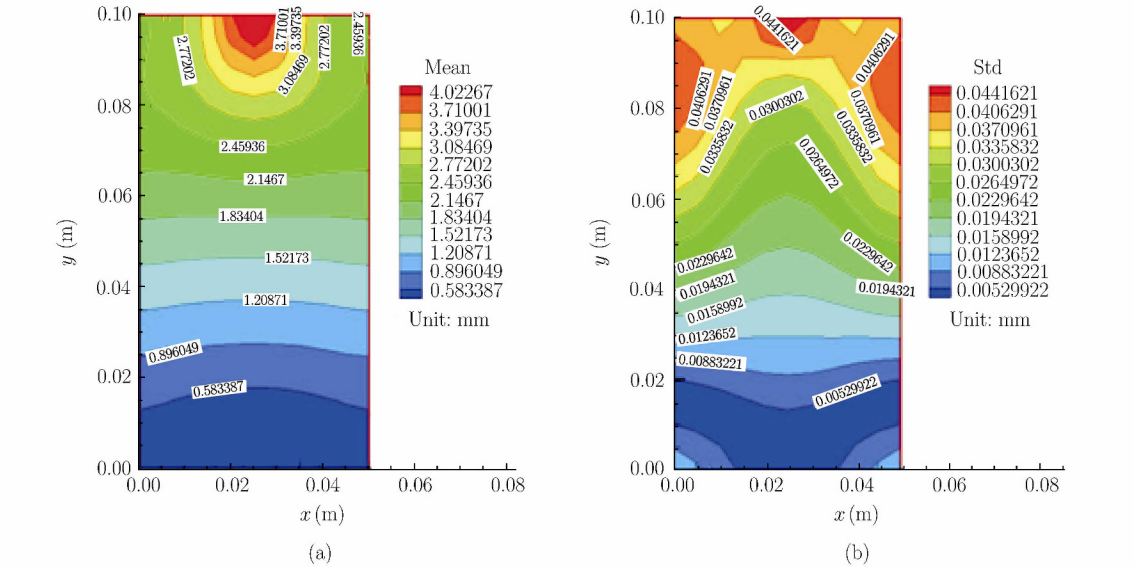

Fig. 8. Second order PCM-5 and its (a) mean value and (b) standard variance (displacement unit: mm).

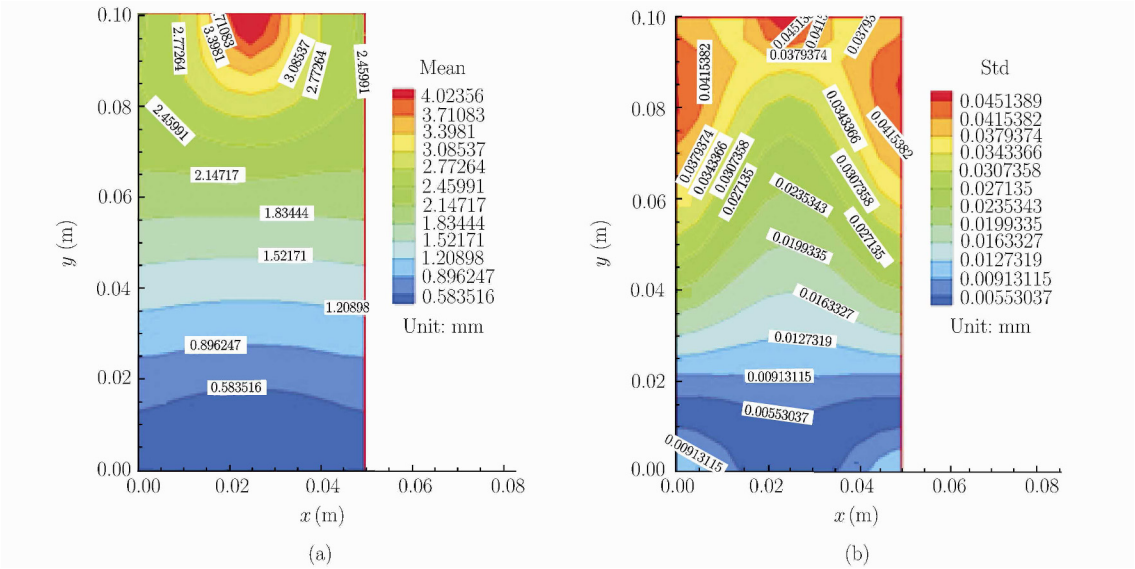

Fig. 9. Second order PCM-10 and its (a) mean and (b) standard variance (displacement unit: mm).

To observe these results in detail, the displacement variations of different expansion terms for section x = 0.025 m are plotted in Fig.13. The mean value of the different PCM expansion items is nearly

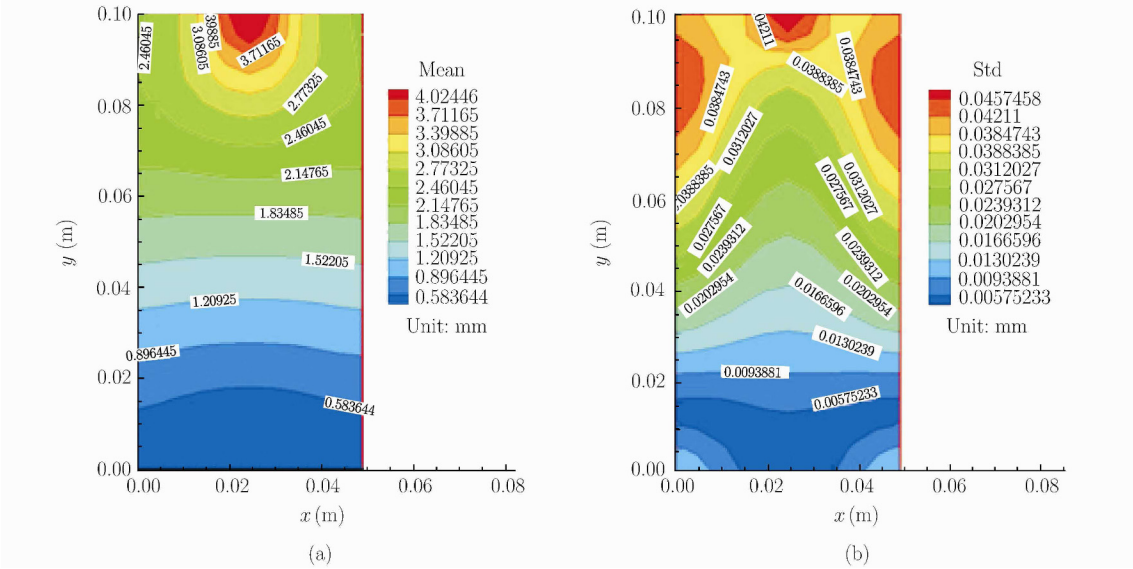

Fig. 10. Second order PCM-20 and its (a) mean and (b) standard variance (displacement unit: mm).

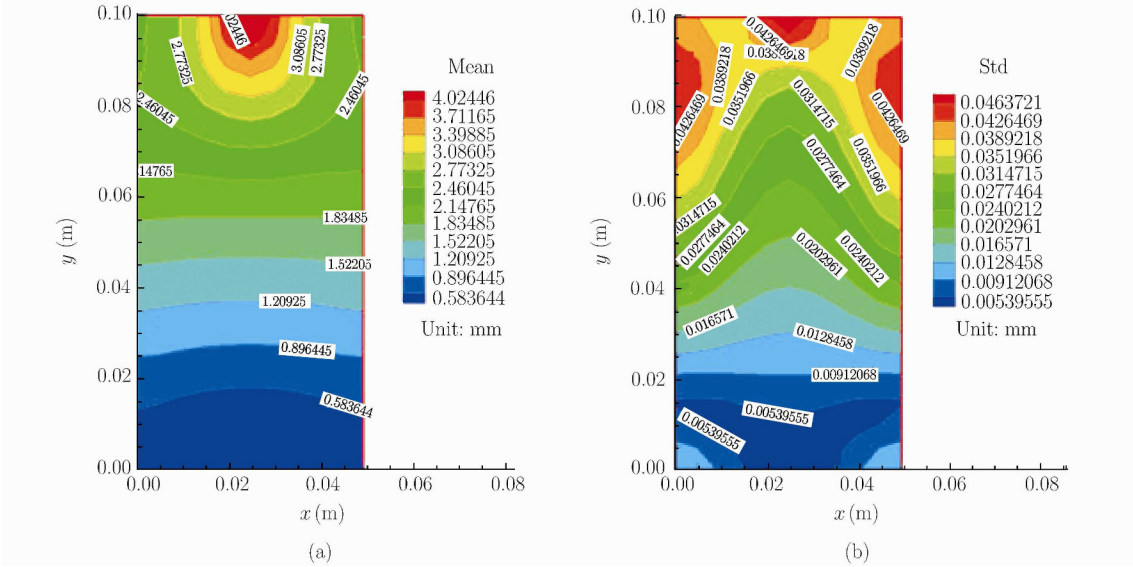

Fig. 11. Second order PCM-30 and its (a) mean and (b) standard variance (displacement unit: mm).

identical. The standard deviation increased with increasing numbers of expansion items. When the expansion item is large enough, the standard deviation is converged.

To show the efficiency of the PCM, the MCS method was used for the same simulations. In the MCS method, a random number is generated using a Gaussian random method. The KL expansion was used to generate the samples, which are then assigned to the material parameters of the rock mass. The numerical EPCA is used to calculate the field variables for each sample. Finally, statistical analysis is performed to obtain the standard deviation and mean values.

We compare the standard deviation between the PCM and MCS at section $x = 0.025$ m. Figure 14 shows that the second order PCM models are consistent with the MCS results for 8000 calculations. For the second order PCE with PCM-20, only 231 (=22!/20!/2!) calculations are needed. However, the MCS results for 231 calculations deviate greatly from those using 8000 calculations. These results indicate the superiority of the PCM, which uses a small number of calculations to obtain high precision for random analysis.

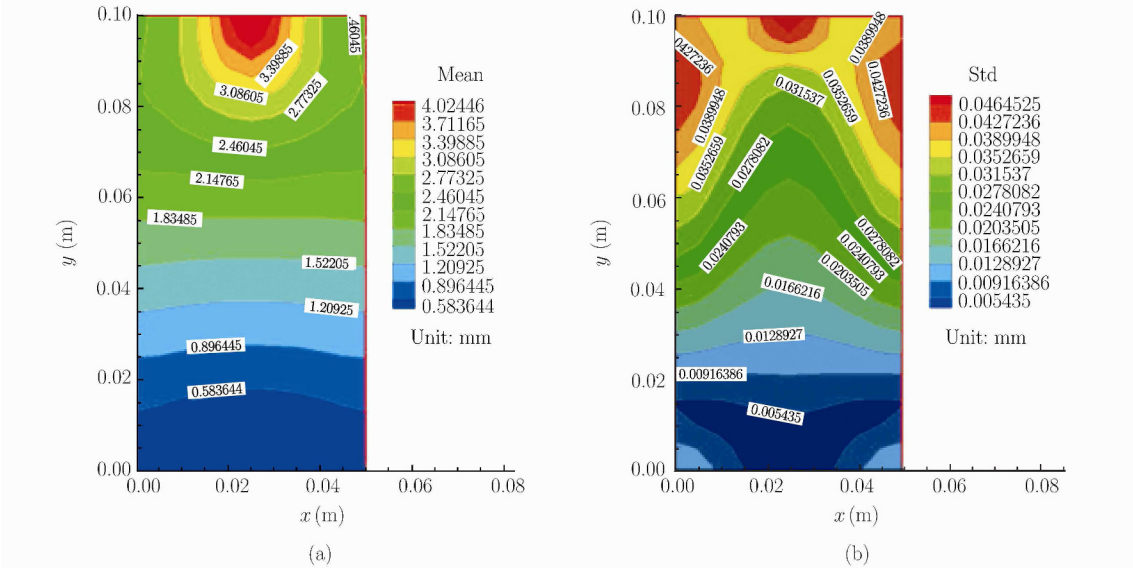

Fig. 12. Second order PCM-40 and its (a) mean and (b) standard variance (displacement unit: mm).

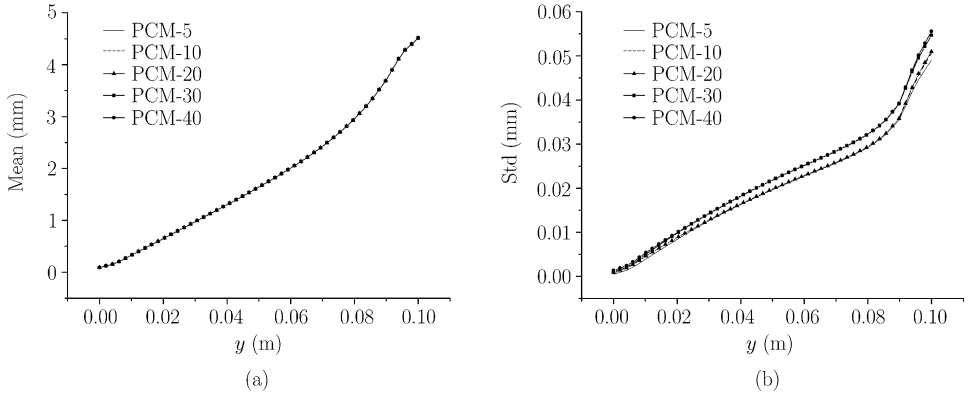

Fig. 13. The (a) mean and (b) standard deviation of the displacement at section $x = 0.025$ m.

For the different input variations (i.e., different coefficients of variation (C.V.)), in the PCM and MCS model (case 1, C.V. = 10%, and case 2, C.V. = 50%), all the input parameters are identical except for case 1 being smaller than case 2. Figure 15 shows the statistics for the displacement at section $x = 0.025$ m, which indicates that the standard deviations obtained from the PCM and MCS for case 1 are almost identical. Again, the PCM uses 231 calculations and obtains results similar to the MCS, which uses 8000 calculations. However, for case 2, the standard deviations differ greatly. The reason for this difference is because increasing the variance in the input domain increases the error from using a low-order PCE to represent the output domain. As a result, the model precision decreases. Additionally, significant deviations may occur. Therefore, the use of a second order PCM can obtain enough precision for calculations from input parameters with small variances. However, for input parameters with large variance, a larger number of expansion terms of KL are required (i.e., PCM-60, 1891 calculations) to be converged with the MCS method, as can be seen from Fig.15(b).

3. Elasto-plastic analysis

The efficiency and reliability of the PCM-EPCA was demonstrated during the elastic analysis. Based on this methodology, elasto-plastic and elasto-brittle-plastic analyses were conducted to study the uncertainty of heterogeneous rock failure behaviour.

Assuming the rock is a perfectly elasto-plastic material, the uncertainty analysis is performed by considering the randomness of the media parameters. The governing equation was expressed using the

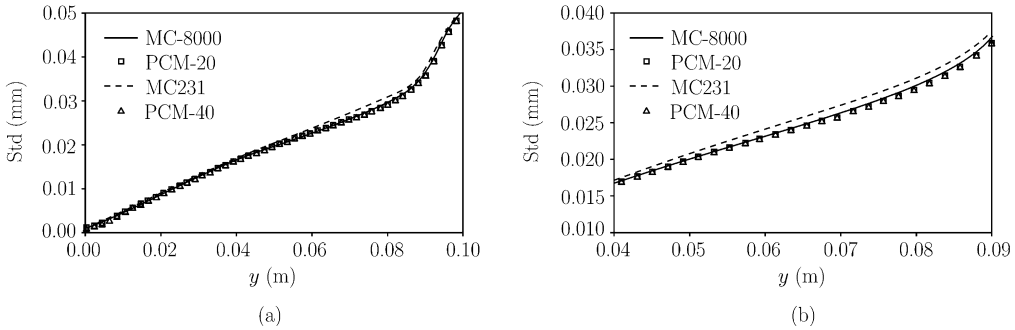

Fig. 14. Comparison of the standard deviation between the PCM and MCS method at section $x = 0.025$ m ((a) an overall view and (b) a close view).

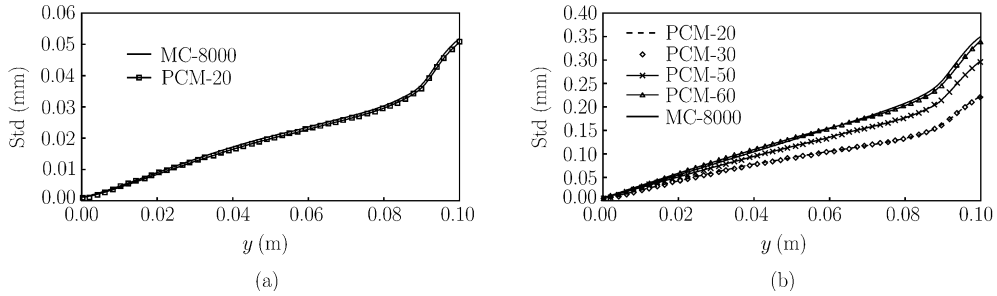

Fig. 15. Comparison between the PCM and MCS models considering the different coefficients of variance. (a) Case 1 C.V $= \sigma/\mu = 10\%$ and (b) Case 2 C.V $= \sigma/\mu = 50\%$.

bulk modulus.

$$\begin{aligned}\frac{3K(1-2\mu)}{(1-\mu^2)}\left(\frac{\partial^2 u}{\partial x^2}+\frac{1-\mu}{2}\frac{\partial^2 u}{\partial y^2}+\frac{1+\mu}{2}\frac{\partial^2 v}{\partial x\partial y}\right)+X=0\\ \frac{3K(1-2\mu)}{(1-\mu^2)}\left(\frac{\partial^2 v}{\partial y^2}+\frac{1-\mu}{2}\frac{\partial^2 v}{\partial x^2}+\frac{1+\mu}{2}\frac{\partial^2 u}{\partial x\partial y}\right)+Y=0\end{aligned} \tag{25}$$

In this model, we use the Mohr-Coulomb yield criterion, which produces the following equation:

$$F(\sigma)=\frac{1}{2}(\sigma_1-\sigma_3)+\frac{1}{2}(\sigma_1+\sigma_3)\sin\phi-c\cos\phi=0 \tag{26}$$

The output field is equivalent to the plastic strain.

$$\bar{\varepsilon}^{\mathrm{p}}=\int\sqrt{\frac{2}{3}\left(\mathrm{d}\varepsilon_1^{\mathrm{p}}\mathrm{d}\varepsilon_1^{\mathrm{p}}+\mathrm{d}\varepsilon_2^{\mathrm{p}}\mathrm{d}\varepsilon_2^{\mathrm{p}}+\mathrm{d}\varepsilon_3^{\mathrm{p}}\mathrm{d}\varepsilon_3^{\mathrm{p}}\right)} \tag{27}$$

We use the PCM to evaluate the uncertainty of an equivalent plastic strain at each node. The numerical model is shown in Fig.7(b).

The bulk modulus is the random input field. The output field is the equivalent plastic strain. The mechanical parameters are assigned according to Table 3.

Table 3. **Mechanical parameters for elasto-plastic analysis**

Mechanical parameters	Bulk modulus		Shear modulus (GPa)	Cohesion (MPa)	Friction angle (°)
	Mean value (Pa)	Variance (Pa^2)			
Value	2.0×10^{11}	4.0×10^{20}	9.8	5	18.5

We use a displacement control method for the uniaxial compression of the rock specimens. The loading rate is 2×10^{-6} m/step. Through a series of trial calculations, the rock specimen exhibits macro-yield within 35 loading steps. Therefore, all of the EPCA simulations have 35 loading steps.

In this model, the different PCM expansion items (PCM-10, PCM-20, PCM-30, PCM-40, and PCM-50) are considered. Figures 16 and 17 show the means and standard deviations of the equivalent plastic strains for PCM-20 and PCM-50 (1326 calculations). It can be observed that the distribution of the means are nearly the same for both cases. The red contour represents the zone with a high equivalent plastic strain. Owing to the heterogeneity of the rock specimen, those places with higher stress or lower strength will yield first during the loading process. These local yield zones lead to the concentration of the stress. The effects of stress adjustment and continuous loading form the macro plastic zone. These results indicate that the red zone has a higher yield probability. Figure 18 shows the statistical behaviour of equivalent plastic strains at section $x = 0.025$ m. Increasing the expansion item decreases the mean value of the equivalent plastic strain, which approaches a convergent value (MCS-8000). The standard deviation increases upon increasing the expansion item and finally reaches a stable state and converges to the MCS method.

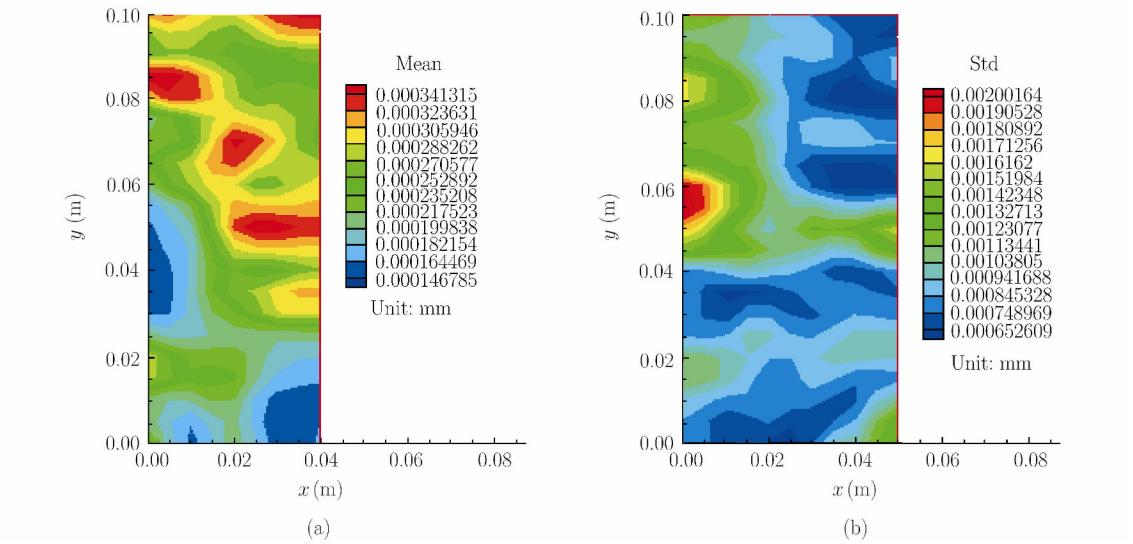

Fig. 16. Statistical results for equivalent plastic strains considering the (a) mean and (b) standard deviation for PCM-20.

The above results for the elasto-plastic analysis are obtained via the statistical analysis of *npc* (*npc* differs for the different expansion items) samples. As a reference, we present 6 typical elasto-plastic model samples. The complete stress-strain curves and associated failure modes (equivalent plastic strain contour) for these samples are shown in Figs.19 and 20, respectively. Although each sample is assigned ideal elasto-plastic properties, their equivalent plastic strain distributions differ from one another. For example, a large plastic strain was found opposite the angle belt in sample 1, which produces a shear. However, sample 5 experiences a split failure. The failure zone of the elasto-plastic materials was not obvious.

4. Elasto-brittle-plastic analysis

An uncertainty analysis is performed using the PCM-EPCA and assuming the rock is an elasto-brittle-plastic material. In this case, the control equation is the bulk modulus (Eq.(25)).

The Mohr-Coulomb theory is used as the yield criterion. The initial yield is expressed as follows:

$$F_i(\sigma) = \frac{1}{2}(\sigma_1 - \sigma_3) + \frac{1}{2}(\sigma_1 + \sigma_3)\sin\phi_i - c_i\cos\phi_i = 0 \tag{28}$$

The residual surface is the following:

$$F_r(\sigma) = \frac{1}{2}(\sigma_1 - \sigma_3) + \frac{1}{2}(\sigma_1 + \sigma_3)\sin\phi_r - c_r\cos\phi_r = 0 \tag{29}$$

The equivalent plastic strain is selected as the output field (Eq.(27)).

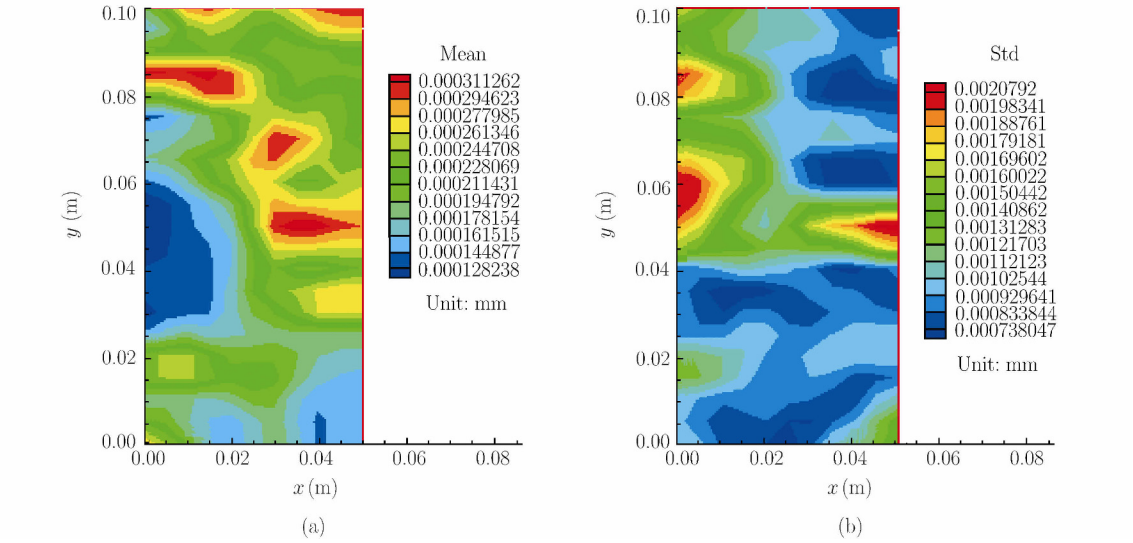

Fig. 17. Statistical results for equivalent plastic strains considering the (a) mean and (b) standard deviation for PCM-50 (elasto-plastic case).

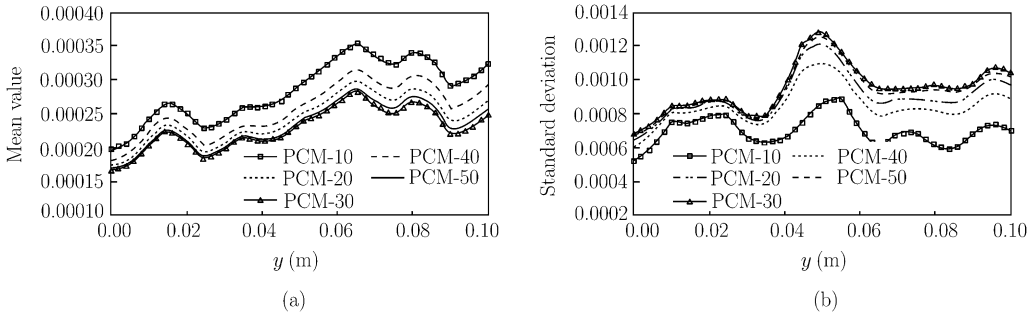

Fig. 18. The (a) mean value and (b) standard deviation for equivalent plastic strains at section $x = 0.025$ m.

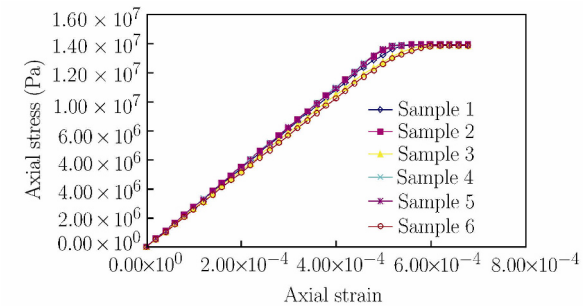

Fig. 19. The complete stress-strain curves for typical samples (elasto-plastic solution).

The numerical model (Fig.7(b)), loading method, loading rate and loading steps are the same as in the previous section. The bulk modulus, shear modulus, initial cohesion and initial friction angle are shown in Table 3. The residual cohesion and residual friction angle are 1 MPa and 6.7°, respectively.

Figures 21∼23 show the results of considering different expansion items (PCM-30, PCM-40 and PCM-50). It can be observed that the distributions of the mean and standard deviation are qualitatively similar. The largest mean and standard deviation for the plastic strain is found in the right lower corner, where the highest failure probability is expected. Figure 24 shows the mean value and standard deviation profile at section $x = 0.025$ m for the different cases. It is found that, increasing the expansion item leads the mean and standard deviation to approach the convergent value with MCS (MC-8000 in Fig.24). The

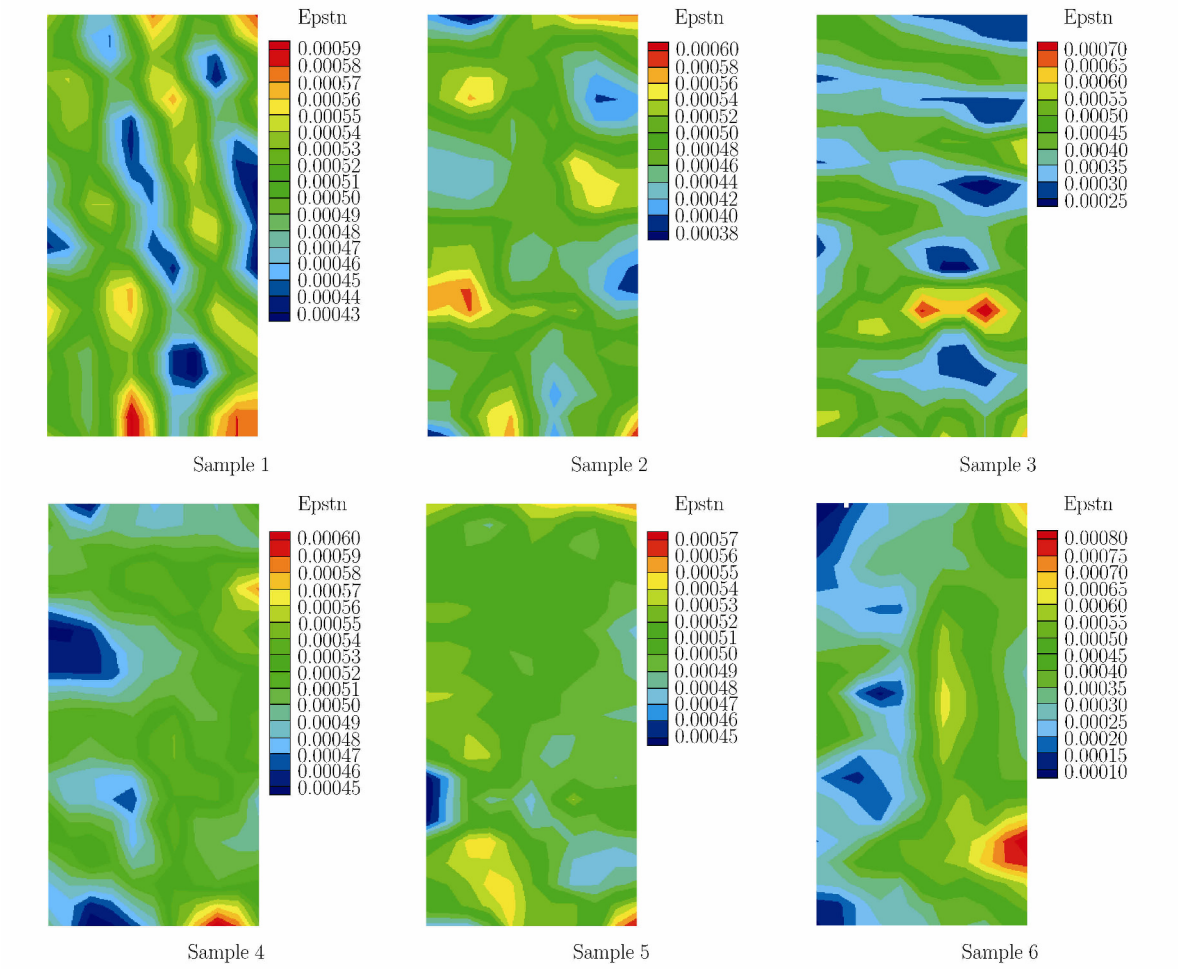

Fig. 20. Distribution of the equivalent plastic strain for typical samples (elasto-plastic solution).

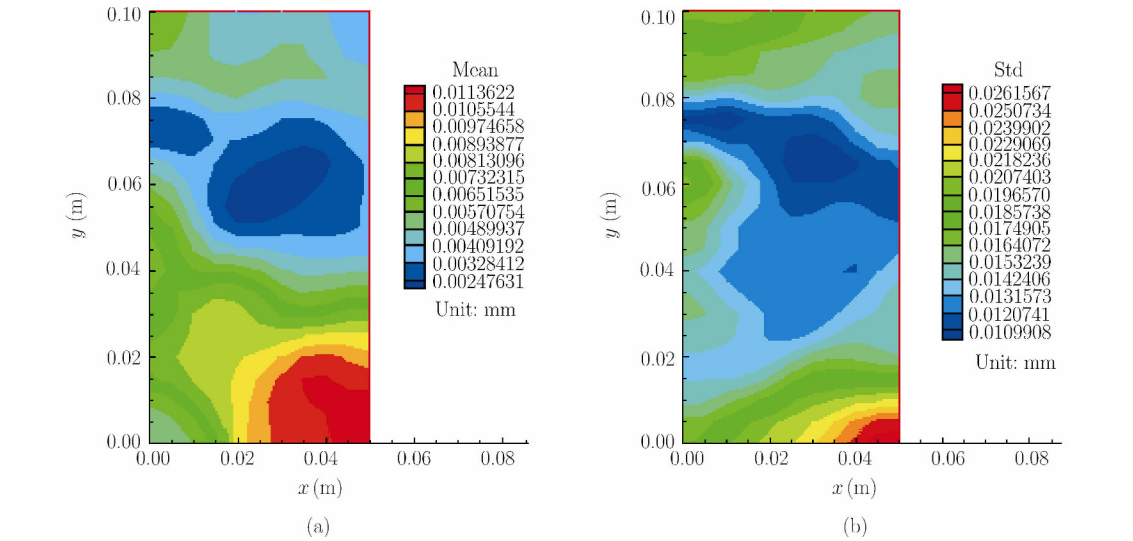

Fig. 21. Statistical results for equivalent plastic strains considering the (a) mean and (b) standard deviation for PCM-30.

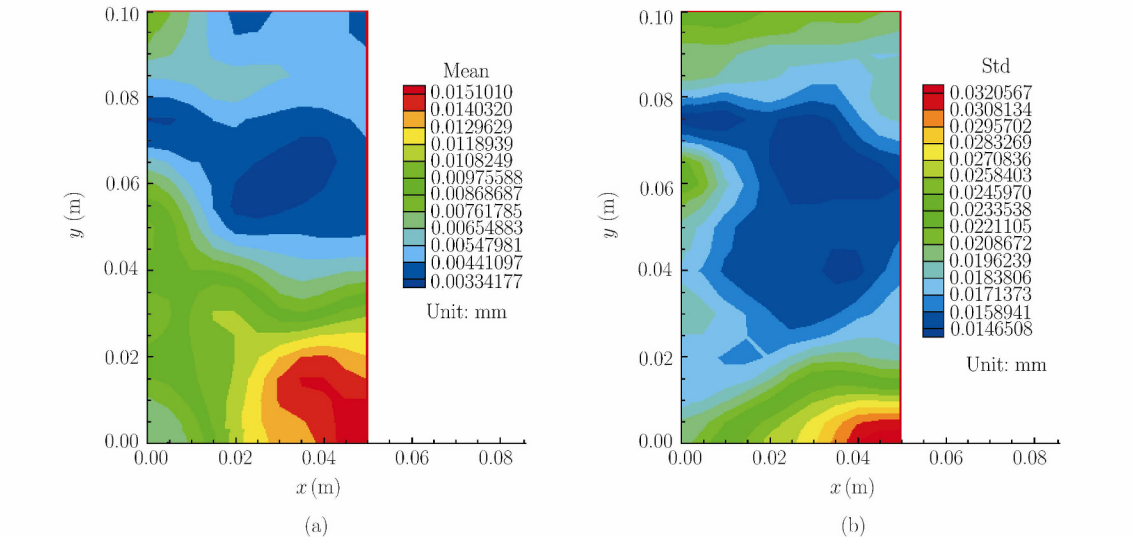

Fig. 22. Statistical results for equivalent plastic strains considering the (a) mean and (b) standard deviation for PCM-40.

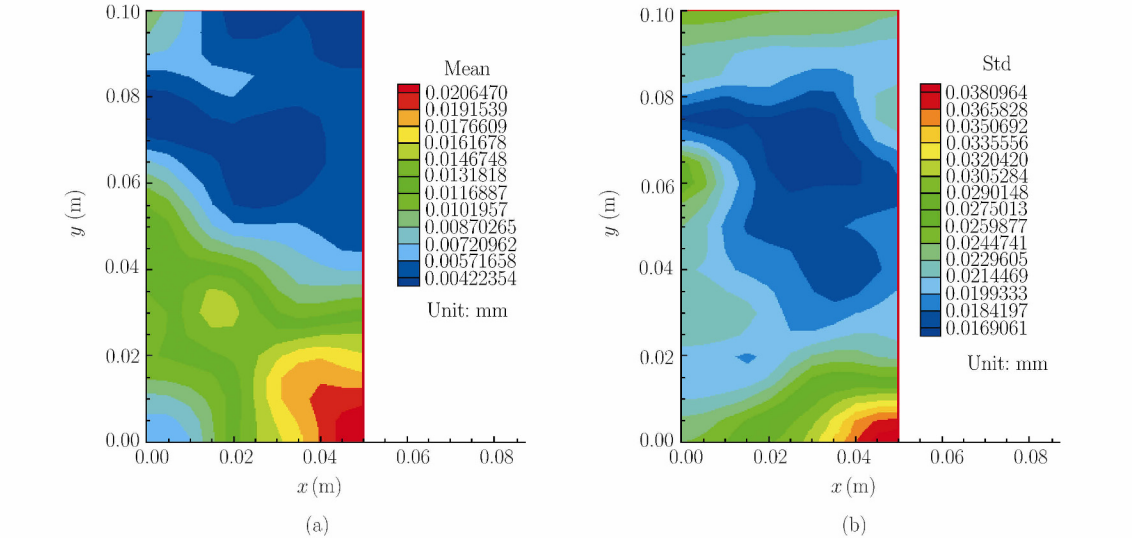

Fig. 23. Statistical results for equivalent plastic strains considering the (a) mean and (b) standard deviation for PCM-50 (elasto-brittle plastic case).

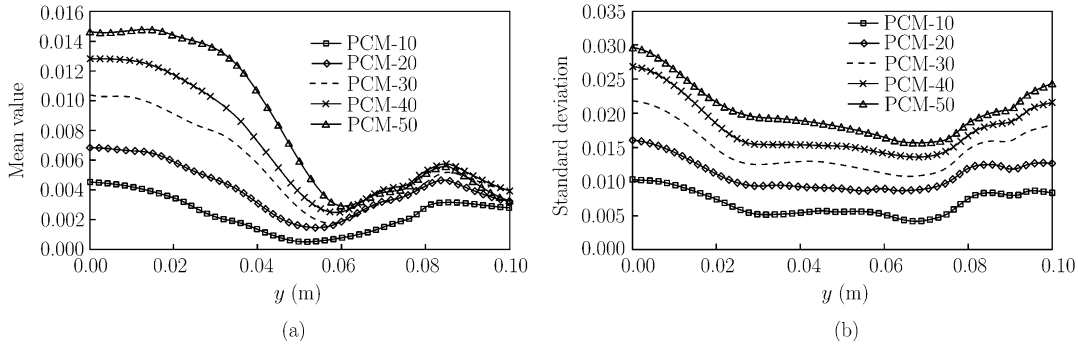

Fig. 24. The (a) mean value and (b) standard deviation of the equivalent plastic strain at section $x = 0.025$ m.

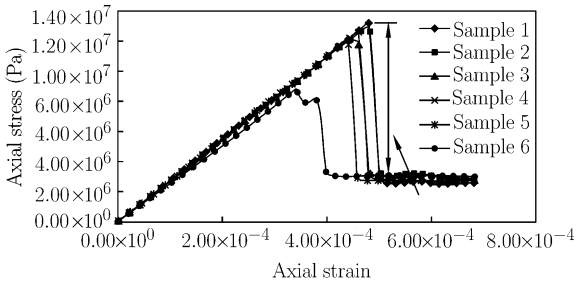

Fig. 25. The complete stress-strain curves of a typical sample (elasto-brittle-plastic solution).

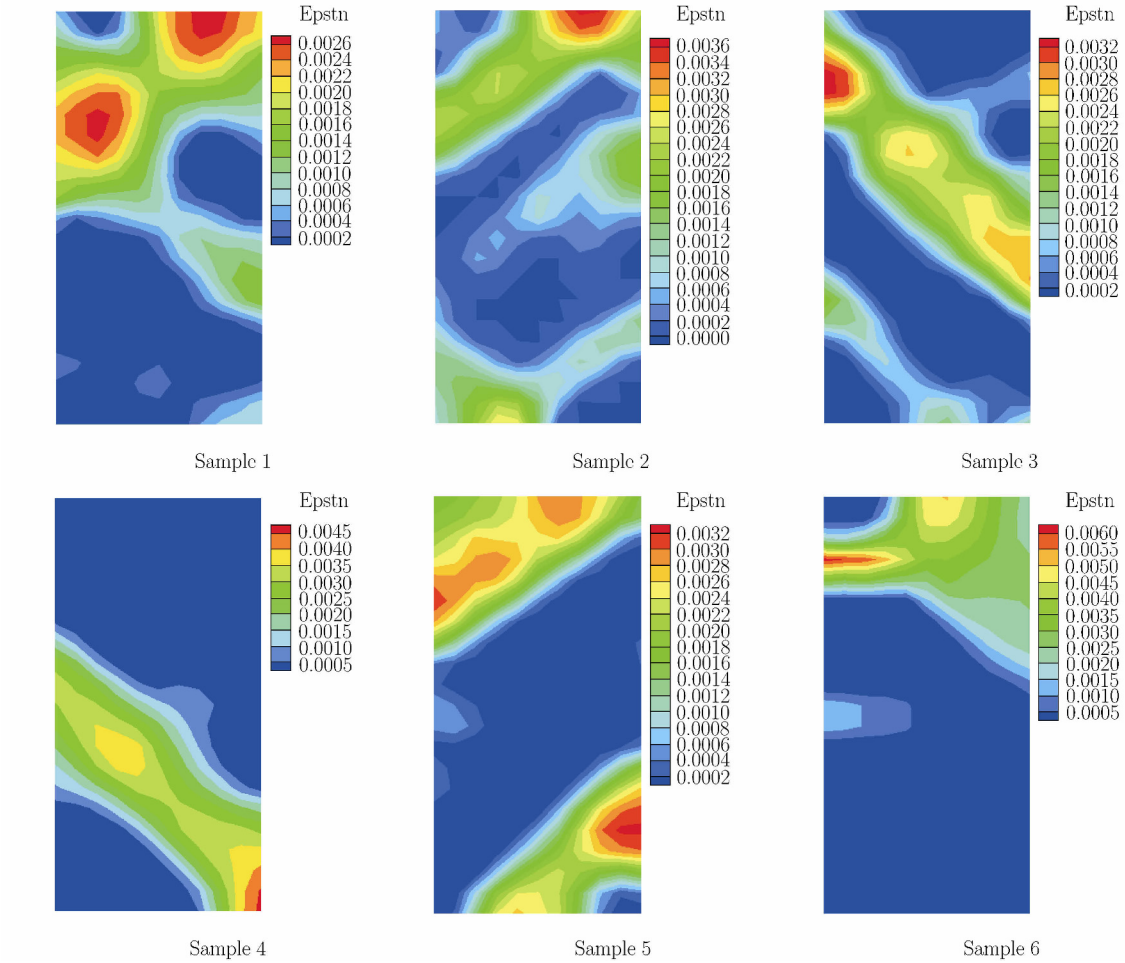

Fig. 26. The distribution of the equivalent plastic strain for a typical sample (elasto-brittle-plastic solution).

convergence speed of the brittle rock is much slower than the elasto-plastic material shown in Fig.18. To obtain more accurate results, the expansion items should be increased. This recommendation means that the failure of brittle rock is less certain, which can be clearly observed from the failure behaviour of the 6 selected samples shown in Figs.25 and 26. Different strength and stiffness are obtained for samples with different heterogeneities. This difference is much larger than that of a perfect elasto-plastic analysis. For the brittle rocks, the localised failure is more serious, and a shear band is clearly found (Fig.26). Energy is stored in the various rock elements during loading and released upon failure. Due to the strong interactions induced by stress redistribution and long-range deformation, the failure of a single important element may cause an avalanche of additional failures in neighbouring elements and lead to a large release of energy. Therefore, for brittle materials, the onset of elemental failure greatly influences

the failure behaviour. For rocks with different heterogeneities, the position where the failure initiates may differ, which directly affects the final failure behaviour of such rocks (Figs.25 and 26).

V. CONCLUSIONS

In this paper, we introduce a method for analysing the uncertainty in the failure behaviour for heterogeneous rock mass by combining the KL expansion and PCM. The PCM is implemented using a self-developed numerical code (i.e., the EPCA), and an uncertainty analysis tool, PCM-EPCA, is developed. This tool is successfully used to analyse the rock failure behaviour considering elastic, elasto-plastic and elasto-brittle-plastic constituents in the rocks. Similar to the MCS method, the PCM also involves sampling. The MCS method, which is based on direct sampling, is conceptually straightforward and easy to implement. Several MCS methods can be very efficient. The main disadvantage of the MCS method is that it uses the law of large numbers to generate a large number of equally probable situations and is thus computationally demanding. The PCM builds an optimal approximation evaluated at selected collocation points and hence reduces the required computational effort significantly. The main advantages of the PCM relative to the MCS method are evident. (1) The random fields are represented by KL expansions with less expansion items required. (2) Using PCM to solve the PCE coefficients and obtain independent certainty equations. This capability greatly reduces the required computational resources. It is convenient to couple this technique with other numerical software for the uncertainty analysis. However, PCM is not always showing its efficiency. In some cases, when a large number of terms are needed in KL expansion, or a high order of PCM is needed, it becomes very inefficient (e.g., the case with high coefficients of variation (C.V.)).

References

[1] Jury,W.A., Simulation of solute transport using a transfer function model. *Water Resources Research*, 1982, 18(2): 363-368.

[2] Yeh,T.C.J., Gelhar,L.W. and Gutjahr,A.L., Stochastic analysis of unsaturated flow in heterogeneous soils: 1. Statistically isotropic media. *Water Resources Research*, 1985, 21(4): 447-456.

[3] Mantoglou,A., A theoretical approach for modeling unsaturated flow in spatially variable soils: Effective flow models in finite domains and nonstationarity. *Water Resources Research*, 1992, 28(1): 251-267.

[4] Russo,D., Stochastic modeling of macrodispersion for solute transport in a heterogeneous unsaturated porous formation. *Water Resources Research*, 1993, 29(2): 383-397.

[5] Tartakovsky,D.M., Neuman,S.P. and Lu,Z., Conditional stochastic averaging of steady state unsaturated flow by means of Kirchhoff transformation. *Water Resources Research*, 1999, 35(3): 731-745.

[6] Zhang,D., Nonstationary stochastic analysis of transient unsaturated flow in randomly heterogeneous media. *Water Resources Research*, 1999, 35(4): 1127-1141.

[7] Zhang,D., Stochastic Methods for Flow in Porous Media: Coping with Uncertainties. Academic Pr., 2002.

[8] Yang,J., Zhang,D. and Lu,Z., Stochastic analysis of saturated-unsaturated flow in heterogeneous media by combining Karhunen-Loeve expansion and perturbation method. *Journal of Hydrology*, 2004, 294(1): 18-38.

[9] Lin,G., Tartakovsky,A.M. and Tartakovsky,D.M., Uncertainty quantification via random domain decomposition and probabilistic collocation on sparse grids. *Journal of Computational Physics*, 2010, 229(19): 6995-7012.

[10] Li,D., Chen,Y., Lu,W. and Zhou,C., Stochastic response surface method for reliability analysis of rock slopes involving correlated non-normal variables. *Computers and Geotechnics*, 2011, 38(1): 58-68.

[11] Li,D.Q., Jiang,S.H. Cheng,Y.G. and Zhou,C.B. A comparative study of three collocation point methods for odd order stochastic response surface method. *Structural Engineering and Mechanics*, 2013, 45(5): 595-611.

[12] Hassan,A.E., Cushman,J.H. and Delleur,J.W., A Monte Carlo assessment of Eulerian flow and transport perturbation models. *Water Resources Research*, 1998, 34(5): 1143-1163.

[13] Ballio,F. and Guadagnini,A., Convergence assessment of numerical Monte Carlo simulations in groundwater hydrology. *Water Resources Research*, 2004, 40(4): W04603.

[14] Zhang,D. and Lu,Z., An efficient, high-order perturbation approach for flow in random porous media via Karhunen-Loeve and polynomial expansions. *Journal of Computational Physics*, 2004, 194(2): 773-794.

[15] Graham,W. and McLaughlin,D., Stochastic analysis of nonstationary subsurface solute transport. *Water Resources Research*, 1989, 25(2): 215-232.

[16] Chen,M., Zhang,D., Keller,A.A. and Lu,Z., A stochastic analysis of steady state two-phase flow in heterogeneous media. *Water Resour. Res*, 2005, 41(1): w01006.

[17] Ghanem,R.G. and Spanos,P.D., Stochastic finite elements: a spectral approach. *Dover Pubns.*, 2003.
[18] Tatang,M.A., Pan,W. Prinn,R.G. and McRae,G.J., An efficient method for parametric uncertainty analysis of numerical geophysical models. *Journal of Geophysical Research*, 1997. 102(D18): 21925-21932.
[19] Feng,X.T., Pan,P.Z. and Zhou,H., Simulation of the rock microfracturing process under uniaxial compression using an elasto-plastic cellular automaton. *International Journal of Rock Mechanics and Mining Sciences*, 2006, 43(7): 1091-1108.
[20] Pan,P.Z., Feng,X.T. and Hudson,J.A., Study of failure and scale effects in rocks under uniaxial compression using 3D cellular automata. *International Journal of Rock Mechanics and Mining Sciences*, 2009, 46(4): 674-685.
[21] Li,H. and Zhang,D. Probabilistic collocation method for flow in porous media: Comparisons with other stochastic methods. *Water Resour. Res*, 2007, 43: 1-13.
[22] Li,H., Accurate and Efficient Uncertainty Quantification of Subsurface Fluid Flow Via the Probabilistic Collocation Method. University of Southern California, 2010.
[23] Ghanem,R., Scales of fluctuation and the propagation of uncertainty in random porous media. *Water Resources Research*, 1998, 34(9): 2123-2136.
[24] Wiener,N., The homogeneous chaos. *American Journal of Mathematics*, 1938, 60(4): 897-936.